JOURNAL OF CATALYSIS 74, 1–8 (1982)

Electronic Structure and Catalytic Activity for N_2O Decomposition on Ni^{2+}, Co^{2+}, and Cr^{3+} in Solid Solutions

A. ANDREEV, E. PROINOV, N. NESHEV, AND D. SHOPOV

Institute of Organic Chemistry, Bulgarian Academy of Sciences, 1113 Sofia, Bulgaria

Received April 23, 1981; revised August 28, 1981

The electron repulsion parameter, B_{35}, obtained from optical spectra is used to describe the electronic state of a transition metal ion in oxide solid solutions. Electronic and catalytic properties are discussed in terms of the correlation between the atomic catalytic activities of transition metal ions and their B_{35} values. Quantum chemical calculations explain the nature of the correlation inherent to the reaction mechanism of N_2O decomposition.

INTRODUCTION

Oxide solid solutions of transition metal ions (TMI) have received considerable attention in fundamental studies of catalytic action over the past 15 years (*1–4*). This has made it possible to enlighten the influence of the TMI electronic configuration, the TMI–TMI interaction, and the effect of the matrix environment, including the local symmetry of the site occupied. N_2O decomposition has been used most frequently as a test reaction for investigations of solid solution catalysts (*1*, *4*) and is covered by this paper.

This work is aimed at introducing the value of the electron repulsion parameter, B_{35}, obtained from optical spectra, as a criterion for TMI electronic state description in the solid solution and at examining the correlation between the catalytic and electronic properties. The mechanism of N_2O decomposition over Ni^{2+}, Co^{2+}, and Cr^{3+} ions in different solid solutions is discussed in terms of B_{35}, based on the results of quantum chemical calculations. The influence of the *d*-electron orbital shape on the adsorbate activation is estimated.

THEORY

Interelectronic Repulsion Parameters

The interelectronic repulsion parameters (IERP) are widely used in atomic and molecular structure theory and spectroscopy (*5*). The energy terms of TMI with $3d^n$ configurations are easily described via the well-known Slater (F_2, F_4) or Racah (B, C) parameters derived from 3*d*-interelectronic repulsion integrals. These parameters are, in general, proportional to the reciprocal localization radius of bound electrons. For the Slater-type atomic orbital, the characteristic electron localization radius is given by

$$r_{\text{loc}}^{-1} \sim \mu = z_*/n_*, \qquad (1)$$

where n_* and z_* are the effective quantum number and the effective charge, respectively.

The nephelauxetic effect (*5*) emphasizes the fact that IERP are smaller in complexes than in the free ion, which is attributed to the radial expansion of the *d* orbitals in the complexes. The so-called "central field covalency" refers to the screening of the nuclear charge by a negative charge of the ligand: $\beta = B(\text{complex})/B(\text{free ion}) \sim z_*(\text{complex})/z_*(\text{free ion})$. "Symmetry-restricted covalency" refers to the delocalization of TMI *d* electrons on the ligand. The MO LCAO description of the complex (O_h symmetry) leads to

$$\tilde{B}_{\text{complex}} \sim N_a^4\, \Phi(\lambda, S_{ML})\, \mu_{nd}, \qquad (2)$$

where $N_a^4 = [1 + \lambda^2 - 2\lambda S_{ML}]^{1/2}$ is a normalizing factor in the antibonding MO with

0021-9517/82/030001-08$02.00/0

dominant $3d$ character, S_{ML} is the group overlap integral, λ the covalency parameter, and μ_{3d}^{-1} is the effective Slater orbital exponent of the bonded TMI.

Taking into account that spin-allowed transitions in the optical spectra are interconfigurational, only the B_{35} parameter is being considered here (the notation B_{35} is related to the notation of $3d$ orbitals in cubic symmetry as 3 (e_g) and 5 (t_{2g})). A review of the numerical procedures for determining B_{35}, on the basis of spectroscopically determined energies of spin-allowed transitions in octahedral and tetrahedral d^3, d^7, and d^8 systems, has been given by Konig (*6*). The B_{35} values used in this paper have been evaluated from reliable experimental data according to Konig's recommendations.

In spite of some minor differences in the interpretation of the physical meaning of the nephelauxetic effect, an agreement exists on the issue that integrals of interelectronic repulsion contain information directly connected with the electronic state of $3d$ electrons in the solid (*7*). It has already been pointed out (*8*) that the Racah parameters can be associated with the extent of electronic isolation of TMI in solid solutions. Due to the smaller metal–oxygen distance in oxides, compared to the aqua complexes, for example, even small changes in the metal–oxygen bond character bring about considerable changes in the B_{35}. The above statements could be deemed as arguments in favour of using the B_{35} parameter as a criterion for characterizing the TMI electronic structure in oxide catalyst systems.

Quantum chemical calculations. Information about the influence of the IERP on the coordinated adsorbate activation has been obtained by model quantum chemical calculations. The calculated electron bond population of the adsorbate in the model has been used as a criterion for its activation.

The variation of the IERP has been modelled by varying the effective exponent μ in the Slater orbital of TMI (Eq. (1)). A proportionality between the IERP (B_{35}) and μ follows from Eq. (2). The interaction between the TMI $3d$ orbitals and the respective adsorbate orbitals is taken into account. The distance between them is taken as the sum of the ionic radius and the adsorbate van der Waals radius. The values of bond populations have been obtained from Mulliken's formula (*9*).

RESULTS AND DISCUSSION

The Correlation between Catalytic Activity and B_{35} Values

Ni^{2+} and Co^{2+} in different host lattices. The N_2O decomposition reaction on Ni^{2+} and Co^{2+} ions in different matrices has been studied in great detail by Cimino and coworkers (*10–16*). The correlation between the atomic catalytic activity (ACA) of nickel ions in N_2O decomposition and the B_{35} value, derived from experimental spectra of catalytic systems under consideration, is given in Fig. 1. The strong effect of Ni^{2+} local-environment symmetry on catalytic activity is demonstrated. It is worth noting that in the case of the $Ni_{0.1}Mg_{0.9}Al_2O_4$ sample the point lies on the correlation line only if the distribution between octahedral and tetrahedral sites is taken into account (*19*).

Similar correlation has been obtained for Co^{2+}-containing systems using appropriate data available such as $Co_xMg_{1-x}O$, $Co_xZn_{1-x}O$, $Co_xMg_{1-x}Al_2O_4$, $Co_xZn_{1-x}Al_2O_4$, and $CoAl_2O_4$. It can now be concluded that the effect of Co^{2+} local environment on the catalytic activity, established firmly by experiment (*22*), manifests itself by corresponding ACA vs B_{35} dependences.

The influence of the TMI environment can be approximated to the effective charge variation in the electrostatic field of the crystal (*25*):

$$z_*^{cryst} = z_* - \left(\pm r_m \frac{z_1\lambda \cdot z_2(\lambda - 1)}{d}\alpha_M\right), \quad (3)$$

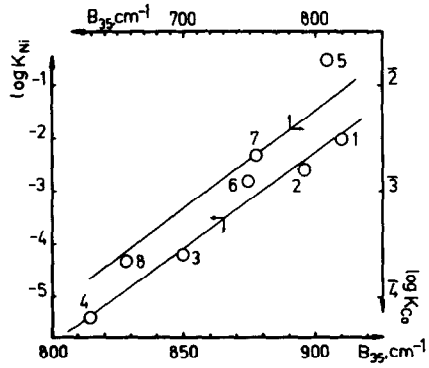

FIG. 1. Atomic catalytic activity (ACA) of Ni^{2+} and Co^{2+} ions in different matrices for N_2O decomposition vs B_{35} values of the catalytic systems: 1—$Ni_{0.1}Mg_{0.9}O$, ACA from (*11*), B_{35} from spectral data in (*17*); 2—$Ni_{0.1}Mg_{0.9}Al_2O_4$, ACA from (*12*), B_{35} from spectral data in (*18*), ion distribution between octahedral and tetrahedral sites from (*19*); 3—$NiAlO_4$, ACA from (*12*), B_{35} from spectral data in (*17*); 4—$Ni_{0.05}Zn_{0.95}O$, ACA from (*13*), B_{35} from spectral data in (*18*) and (*20*); 5—$Co_{0.01}Mg_{0.99}O$, ACA from (*15*), B_{35} from (*21*); 6—$Co_{0.04}Mg_{0.96}Al_2O_4$, ACA from (*22*), B_{35} from spectral data in (*23*) (distribution between octahedral and tetrahedral sites taken into account (*22*)); 7—$CoAl_2O_4$, ACA from (*22*), B_{35} from spectral data in (*23*); 8—$Co_{0.01}Zn_{0.99}O$, ACA from (*24*), B_{35} from (*6*).

where z_1, z_2 are the cation and anion charges, d the distance between ions, α_M the Madelung constant, λ the degree of the Me–O bond covalency, and $r_m = a_H n_*^2/z_*$ is the distance between the nucleus and the 3*d*-electron density maximum. According to Eq. (3) the influence of the TMI environment on B_{35} (proportional to z_*^{cryst}, see Eq. (2)) is directly introduced by particular α_M and d values of the crystal. The chemical individuality of the TMI is represented by r_m.

Ni^{2+}, Co^{2+}, and Cr^{3+} ions dispersed in different concentrations. The ACA in the N_2O decomposition reaction has been studied for Ni^{2+} and Co^{2+} in magnesium oxide (*11, 15*), zinc oxide (*13, 24*), and some spinel systems (*10, 12, 22*). A "dilution effect," i.e., an increase in ACA when concentration decreases, has been found for all the systems studied.

Experimental ACA for N_2O decomposition over Ni^{2+}- and Co^{2+}-containing magnesium oxide samples have been analysed based on reliable spectral data available for B_{35}. Figure 2 shows a good correlation between the ACA and the corresponding B_{35} values for both nickel- and cobalt-containing magnesia. As observed earlier (Fig. 1), higher catalytic activity corresponds to higher B_{35} values in both series.

The variation of N_2O decomposition activity with TMI concentration has been studied on $Al_{2-x}Cr_xO_3$ (*27, 28*) andd Mg $Al_{2-x}Cr_xO_4$ (*29*) for the whole range of compositions (x = 0–2). Interest in these systems is aroused by the possibility of studying cation–cation interaction in concentrated solid solutions (*8, 30*). The results of the ACA vs B_{35} dependence for $Al_{2-x}Cr_xO_3$ are presented in Fig. 3. As in the case of diluted nickel- and cobalt-containing systems, a small increase of B_{35} enhances the activity in the region of diluted solutions but a reverse activity rise is observed in concentrated samples. This interesting feature will be discussed later.

There is no full agreement on the issue of B_{35} dependence on chromium concentration in $Al_{2-x}Cr_xO_3$. Many attempts have been made to explain it by the Cr^{3+}-site geometry changes and Cr^{3+}–Cr^{3+} interaction between π-antibonding t_{2g} electrons (*31*). More acceptable explanations, in

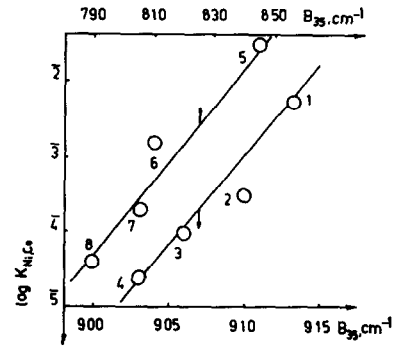

FIG. 2. ACA of Ni^{2+} and Co^{2+} ions in MgO vs B_{35} values. $Ni_xMg_{1-x}O$: 1—x = 0.01, 2—x = 0.1, 3—x = 0.2, 4—x = 0.5; ACA ($\log k_{Ni}$ at 713 K) from (*11*); B_{35} calculated from spectral data in (*17*). $Co_xMg_{1-x}O$: 5—x = 0.01, 6—x = 0.1, 7—x = 0.2, 8—x = 0.5; ACA ($\log k_{Co}$ at 588 K) from (*15*); B_{35} from (*21, 26*).

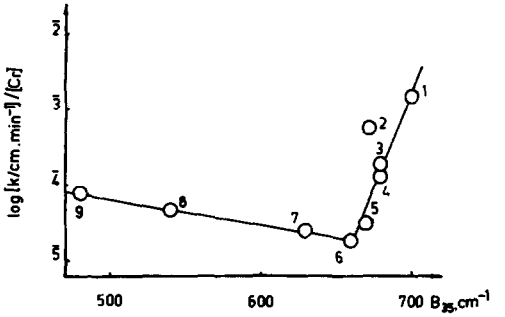

FIG. 3. ACA of Cr^{3+} ions for N_2O decomposition vs B_{35} values for $Al_{2-x}Cr_xO_3$: 1—$x = 0.020$, 2—$x = 0.054$, 3—$x = 0.068$, 4—$x = 0.098$, 5—$x = 0.182$, 6—$x = 0.400$, 7—$x = 0.794$, 8—$x = 1.200$, 9—$x = 2.00$; ACA (log k_{Cr} at 555 K) from (*26*); B_{35} from (*29*) (for Cr_2O_3 another widely accepted value from (*31*)).

agreement with X-ray and magnetic data, could be given in terms of Cr–O bond covalency changes with concentration. The sensitivity of B_{35} to covalency changes is evident from Eqs. (2) and (3). The interaction between strongly connected polyhedra in the corundum structure determines the sensitivity of the Cr^{3+} electronic state to chemical changes in its environment. A similar effect of the concentration on B_{35} has been observed for $Ni_xMg_{1-x}O$ and $Co_xMg_{1-x}O$ (*16, 20, 32*).

TMI with different electronic configurations. The only data available for the relative activity of first-series TMI solid solutions are those summarised by Cimino (*1*). Comparison of the activities for N_2O decomposition on 1% solid solutions at 315°C is made, involving ions with configurations from d^3 to d^9. Only catalytic activity data (log k_{abs}) which are not subjected to error due to the presence of ions with different valencies will be considered. The catalytic activities and the most reliable IERP are given in Table 1. β_{35} instead of B_{35} values are used as more appropriate when comparing the properties of TMI with different electronic configurations.

There are other parameters available for describing the relativistic nephelauxetic effect (*5*) ensuing from the g factor obtained by EPR data (*33*). The g factor for octahedral complexes of d^3 and d^8 configurations can be written as

$$g = 2.00229 - 8\lambda_{nd}/Dq \quad \text{and} \quad g = 2.00229 + 4\lambda_{nd}/Dq,$$

where λ_{nd} is the spin–orbit coupling constant. The $\lambda_{nd}/\lambda_{nd}^0$ (λ_{nd}^0 refers to the gaseous ion) is proportional to the effective charge in the crystal.

TABLE 1

Catalytic Activity and Some Physical Constants for TMI in MgO

Ion	Catalytic activity of 1% solid solution in MgO, log k_a (315°C)	β_{35}	g value[a]	λ/λ_0 from EPR data[b]	R[c]	ΔE[d] (eV)
Co^{2+}	−2.38	0.87[e]	4.2785	0.85	1.40	1.7
Ni^{2+}	−3.12	0.79[f]	2.2145	0.77	1.25	1.7
Cu^{2+}	−4.12	—	2.190	—	—	—
Cr^{3+}	−4.34	0.67[g]	1.9782	0.72	1.29	2.2
Fe^{3+}	−5.21	—	2.0037	—	1.15	4.4

[a] Ref. (*33*).
[b] Ref. (*34*).
[c] Ref. (*25*).
[d] Ref. (*36*).
[e] Ref. (*26*).
[f] Ref. (*35*).
[g] Ref. (*31*).

As indicated in Table 1, the catalytic activity for N_2O decomposition is markedly influenced by the cation electronic structure. Maximum activity is reached for ions with maximum β_{35} and $\lambda_{nd}/\lambda_{nd}^0$ values. In agreement with earlier findings for diluted systems, higher catalytic activity corresponds to higher electron localization on the ion.

Intraatomic electron interaction (electron correlation) is a decisive factor in determining TMI properties in the free state as well as in the solid phase (*37*). In order to estimate the atomic-orbital energies, Slater (*37*) proposed the use of "modified one-electron energies":

$$E'_i = I(i) + (q_i - \tfrac{1}{2})(i, i) + \sum_{i=j} q_j(i, j), \quad (4)$$

where $I(i)$ is the sum of the kinetic and potential energies of an electron in the ith orbital in the nucleus field, (i, i) is the electrostatic interaction integral between two electrons in the orbital i, (i, j) is the interaction integral between an electron in the ith shell and one in the jth shell, and q is the occupation number of the shell. These E'_i values have been successfully used in solid state electronic structure descriptions (*37*). The configurational stability of the 3*d*-electronic state can be evaluated taking into account the spin polarization with the quantities $\bar{E}'_i = (q_\uparrow E'_{i\uparrow} + q_\downarrow E'_{i\downarrow})/q$, where $q = q_\uparrow + q_\downarrow$. The corresponding $\bar{E}'_{3d}$ values for different 3*d* configurations have been obtained using $E'_{3d_\uparrow}$ and $E'_{3d_\downarrow}$ data for $3d^n s^2$ (*38*):

Configuration	$3d^3$	$3d^5$	$3d^7$	$3d^8$	$3d^9$
$\bar{E}'_{3d}$ (Ry)	−0.500	−0.550	−0.488	−0.494	−0.517

Comparison between $\bar{E}'_{3d}$ values (as a measure of configurational stability) and TMI catalytic activity (Table 1) reveals a reverse correlation between them: a highly active TMI possesses more unstable ("quick" in a chemical sense) 3*d* shells due to a higher interelectron repulsion.

The high sensitivity of TMI polarizability (α) to the effective charge $-\partial\alpha/\alpha = 4\partial z_*/z_*$ (*24*) confirms the relationship between reactivity and interelectron repulsion. The refractions (R) of TMI, presented in Table 1, correlate with catalytic activity. The fact that polarizability reflects "liquidity" of 3*d*-electron density, caused by the high effective charge value, explains this relationship.

The influence of the Coulomb and the exchange components of intraatomic electron interaction on the TMI can be estimated also by the energy difference (ΔE) between the ground and the first excited states (ΔE is listed in Table 1). As indicated in Table 1, the cations with smaller excitation energy possess higher catalytic activity.

The above arguments help to gain further insight into the correlation between the ACA and the IERP. It is also possible to explain the "*d*-correlation effect" (*39*) on the same basis. However, it has to be kept in mind that a mainly independent TMI in a solid solution is being considered here and that electron delocalization in concentrated solutions or pure oxides requires special treatment.

An interesting interpretation of the activity on oxide solid solution systems was given by Pomonis and Vickerman (*40*), based on the effective size of the electronic trap. It must be pointed out in connection with the present results that the effective size of the electronic trap is proportional to the interelectronic interaction on the TMI.

B_{35} *Values and Reaction Mechanism*

According to the data presented so far, there exists a correlation between the catalytic activity and the corresponding B_{35} values of the samples. An attempt will now be made to connect the electronic state of the TMI and the mechanism of the catalytic reaction on the basis of the B_{35} concept.

The mechanism of N_2O decomposition is known to a certain extent and it has been concluded "that the nature of the surface complex between oxygen and the metal ion

controls the course of the reaction" (*1*):

$$N_2O(g) \rightarrow N_2O(ads), \quad (5)$$

$$N_2O(ads) + e^- \rightarrow N_2O^-(ads), \quad (6)$$

$$N_2O^-(ads) \rightarrow N_2(g) + O^-(ads), \quad (7)$$

$$O^-(ads) \rightarrow \tfrac{1}{2}O_2(g) + e^-. \quad (8)$$

If the desorption step (Eq. (8)) is rate determining, the higher activity can be attributed to the weaker TMI–oxygen bond.

Quantum chemical calculations of the Me–O bond order (P_{M-O}) have been carried out with orbital exponent μ variation, thus modelling TMI with different B_{35} values, according to Eq. (2). The parameter μ has been varied within reasonable limits, in line with the modern concepts of chemical bonding (*41*). Figure 4 depicts P_{Cr-O} and P_{Co-O} values as a function of μ. In the same figure the ACA/B_{35} dependence for $Cr_xAl_{2-x}O_3$ and $Co_xMg_{1-x}O$ is shown at a fixed proportion between μ and B_{35}. The corresponding Slater orbital exponents and B_{35} values for free (gaseous) Cr^{3+} and Co^{2+} ions have been used as fixing points between μ and B_{35} axes.

The higher catalytic activity of Co^{2+} at higher B_{35} values corresponds to a lower P_{Co-O} value (Fig. 4), i.e., a weaker Co–O bond facilitates oxygen desorption and enhances catalytic activity. The minimum in ACA/B_{35} dependence observed for $Cr_xAl_{2-x}O_3$ coincides with the maximum in the P_{Cr-O}/μ curve also in agreement with the mechanism in Eqs. (5)–(8). It is evident that the orbital shape individuality (expressed by the appropriate μ value) specifically influences the electron density distribution in the adsorption complex and hence the reaction mechanism.

The model used for the present quantum chemical calculations is based on the concept that the *d* levels localized on the metal cation exist in the oxide systems under consideration (*42*). The EHM calculations of Me–O bond populations (Fig. 4) have been carried out with a fixed diagonal matrix element H_{3d} (representing localized 3*d* levels) for different μ values. The H_{3d} values have been chosen according to existing data for impurity 3*d* levels in the oxide solid solution (*42*). The 3*d*-electron energy level depends, however, upon interelectronic interaction (see Eq. (4)). In specially performed quantum chemical calculations of P_{Cr-O}/μ curves for different H_{3d} it has been proved that the general mode of P_{Cr-O}/μ dependence does not change with reasonable H_{3d} variation (Fig. 5). It would be reasonable to

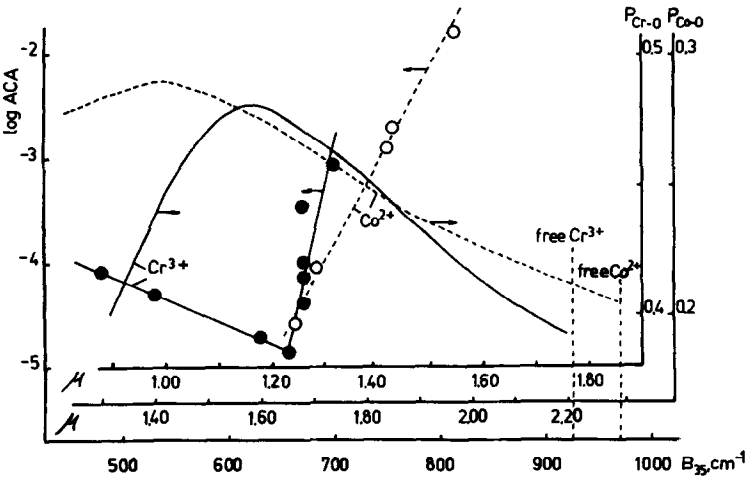

FIG. 4. The Me–O bond population (P_{M-O}) calculated quantum chemically as a function of the μ value. ACA/B_{35} dependences from Figs. 1 and 3.

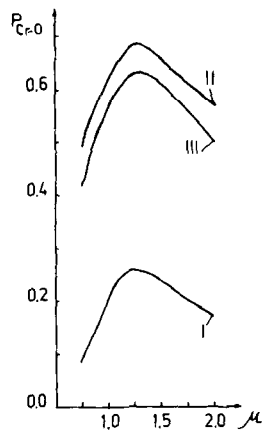

FIG. 5. The Cr–O bond population (P_{Cr-O}) calculated quantum chemically as a function of the μ value at different H_{3d}: I—$H_{3d} = -7.00$ eV, II—$H_{3d} = -13.00$ eV, III—$H_{3d} = -20.00$ eV ($H_{2p}^{O} = -15.07$ eV, $\mu_{2p} = 2.25$).

assume that conclusions concerning the reaction mechanism could be drawn on the basis of Fig. 4 irrespectively of the choice of H_{3d} value.

According to the calculation method used, the covalency of the Me–O bond is proportional to the corresponding bond population. The maximum covalency of the Cr–O bond is shown in Fig. 5, curve II, for which the condition $H_{3d_{Cr}} \sim H^{2pO}$ is fulfilled, while curves I and III reveal greater ionicity: $H_{3d}^{Cr} < H_{2p}^{O}$ and $H_{3d}^{Cr} > H_{2p}^{O}$, respectively. This reveals the possibility of estimating the influence of the Me–O covalency within such a model.

The model quantum chemical calculations carried out are qualitative and the conclusions drawn on them are within the limits of the EHM.

CONCLUSIONS

The B_{35} parameter of interelectronic repulsion defines the electronic properties of TMI in solid solutions. Correlation between the ACA for N_2O decomposition and B_{35} is found and satisfactorily explained by quantum chemical calculations based on the effective charge concept, in accordance with the experimentally substantiated mechanism. It seems that the experimentally obtained B_{35} is an objective and informative criterion for characterizing the electronic properties of TMI-containing catalysts. This treatment demonstrates the opportunities offered by the interelectronic repulsion concept for studying the mechanism of TMI catalytic activity in solid solutions.

REFERENCES

1. Cimino, A., *Chim. Ind. (Milan)* **56,** 27 (1974).
2. Stone, F. S., *J. Solid State Chem.* **12,** 271 (1975).
3. Boreskov, G. K., *in* "Proceedings, 6th International Congress on Catalysis, London, 1976" (G. C. Bonds, P. B. Wells and F. C. Tompkins, Eds.), Vol. 1, p. 204. The Chemical Society, London, 1977.
4. Vickerman, J. C., *in* "Catalysis," Vol. 2, p. 107. Specialist Periodical Report, The Chemical Society, London, 1978.
5. Jorgensen, C. K., *Advan. Chem. Phys.* **5,** 33 (1963); *in* "Structure and Bonding" (J. D. Dunitz *et al.*, Eds.), Vol. 1, p. 3. Springer-Verlag, Berlin/Heidelberg/New York, 1966.
6. Konig, E., *in* "Structure and Bonding" (J. D. Dunitz *et al.*, Eds.), Vol. 9, p. 175. Springer-Verlag, Berlin/Heidelberg/New York, 1972.
7. Brandow, B. H., *Advan. Phys.* **26,** 651 (1977).
8. Stone, F. S., and Vickerman, J. C., *Trans. Faraday Soc.* **67,** 316 (1971).
9. Mulliken, R. S., *J. Chem. Phys.* **23,** 1833 (1955).
10. Cimino, A., Indovina, V., Pepe, F., and Schiavello, M., *Zh. Fiz. Khim.* **52,** 2890 (1979).
11. Cimino, A., Indovina, V., Pepe, F., and Schiavello, M., *J. Catal.* **14,** 49 (1969).
12. Cimino, A., and Schiavello, M., *J. Catal.* **20,** 202 (1971).
13. Schiavello, M., Cimino, A., and Criado, J., *Gazz. Chim. Ital.* **101,** 47 (1971).
14. Schiavello, M., Lo Jacono, M., and Cimino, A., *J. Phys. Chem.* **75,** 1051 (1971).
15. Cimino, A., and Pepe, F., *J. Catal.* **25,** 362 (1972).
16. Indovina, V., Cimino, A., Inversi, M., and Pepe, F., *J. Catal.* **58,** 396 (1979).
17. Reinen, D., *Ber. Bunsenges. Phys. Chem.* **69,** 82 (1965).
18. Schmitz-Du Mont, O., Lulé, A., and Reinen, D., *Ber. Bunsenges. Phys. Chem.* **69,** 76 (1965).
19. Porta, P., Stone, F. S., and Turner, R. G., *J. Solid State Chem.* **11,** 135 (1974).
20. Reinen, D., *Z. Anorg. Allg. Chem.* **37,** 238 (1964).
21. Reinen, D., *Mh. Chem.* **96,** 730 (1965).
22. Angeletti, C., Pepe, F., and Porta, P., *J. Chem. Soc. Faraday Trans. 1* **74,** 1595 (1978).
23. Ashley, J. H., and Mitchell, P. C. H., *J. Chem. Soc. A,* 2821 (1968).
24. Pepe, F., Schiavello, M., and Ferreris, G., *Z. Phys. Chem. Neue Folge* **96,** 297 (1975).

25. Batsanov, S. S., and Zvyagina, R. A., "Overlap Integrals and Problem of Effective Charges." Nauka, Novosibirsk, 1966. [Russian].
26. Pappalardo, R., Wood, D. L., and Linares, R. C., Jr., *J. Chem. Phys.* **35,** 2041 (1961).
27. Egerton, T. A., Stone, F. S., and Vickerman, J. C., *J. Catal.* **33,** 299 (1974).
28. Egerton, T. A., Stone, F. S., and Vickerman, J. C., *J. Catal.* **33,** 307 (1974).
29. Egerton, T. A., and Vickerman, J. C., *J. Catal.* **19,** 74 (1970).
30. Vickerman, J. C., *Trans. Faraday Soc.* **67,** 665 (1971).
31. Reinen, D., *Struct. Bonding* **6,** 30 (1969).
32. Reinen, D., *Z. Naturforsch. A* **23,** 521 (1968).
33. Wertheim, G. K., Hausmann, A., and Sander, W., "The Electronic Structure of Point Defects." North-Holland, Amsterdam/London, 1971.
34. Low, P., "Paramagnetic Resonance in Solids. Solid State Physics, Suppl. 2." Academic Press, New York/London, 1960.
35. Pappalardo, R., Wood, L. D., and Linares, R. C., Jr., *J. Chem. Phys.* **35,** 1460 (1961).
36. Bersuker, J. B., "Electronic Structure and Properties of Coordination Compounds." Chimia, Leningrad, 1976. [Russian.]
37. Slater, J., *Int. J. Quantum Chem.* **IIIS,** 727 (1970).
38. Slater, J., Mann, J., Wilson, T., and Wood, J., *Phys. Rev.* **184,** 672 (1969).
39. Dowden, D. A., and Wells, D., *in* "Actes du Deuxième Congrès International de Catalyse, Paris, 1960," Vol. 2, p. 1489. Editions Technip, Paris, 1961.
40. Pomonis, P., and Vickerman, J. C., *J. Catal.* **55,** 88 (1978).
41. Ruedenberg, K., *in* "Localization and Delocalization in Quantum Chemistry" (O. Chalvet, R. Daudel, S. Diner, and J. P. Malrieu, Eds.), Vol. I. Reidel, Dordrecht/Holland, 1975.
42. Andreev, A., and Shopov, D., "Chemical Bonding in Adsorption and Catalysis. II. Oxides." Publ. House Bulg. Acad. Sci., Sofia, 1979. [Russian.]